Structure, Vol. 9, 987–997, October, 2001, ©2001 Elsevier Science Ltd. All rights reserved. PII S0969-2126(01)00661-X

# Crystal Structure of Imidazole Glycerol Phosphate Synthase: A Tunnel through a $(\beta/\alpha)_8$ Barrel Joins Two Active Sites

**Barnali N. Chaudhuri,[1,4] Stephanie C. Lange,[1,5] Rebecca S. Myers,[2] Sridar V. Chittur,[2] V. Jo Davisson,[2] and Janet L. Smith[1,3]**
[1] Department of Biological Sciences
[2] Department of Medicinal Chemistry and Molecular Pharmacology
Purdue University
West Lafayette, Indiana 47907

## Summary

**Background:** Imidazole glycerol phosphate synthase catalyzes a two-step reaction of histidine biosynthesis at the bifurcation point with the purine de novo pathway. The enzyme is a new example of intermediate channeling by glutamine amidotransferases in which ammonia generated by hydrolysis of glutamine is channeled to a second active site where it acts as a nucleophile. In this case, ammonia reacts in a cyclase domain to produce imidazole glycerol phosphate and an intermediate of purine biosynthesis. The enzyme is also a potential target for drug and herbicide development since the histidine pathway does not occur in mammals.

**Results:** The 2.1 Å crystal structure of imidazole glycerol phosphate synthase from yeast reveals extensive interaction of the glutaminase and cyclase catalytic domains. At the domain interface, the glutaminase active site points into the bottom of the $(\beta/\alpha)_8$ barrel of the cyclase domain. An ammonia tunnel through the $(\beta/\alpha)_8$ barrel connects the glutaminase docking site at the bottom to the cyclase active site at the top. A conserved "gate" of four charged residues controls access to the tunnel.

**Conclusions:** This is the first structure in which all the components of the ubiquitous $(\beta/\alpha)_8$ barrel fold, top, bottom, and interior, take part in enzymatic function. Intimate contacts between the barrel domain and the glutaminase active site appear to be poised for crosstalk between catalytic centers in response to substrate binding at the cyclase active site. The structure provides a number of potential sites for inhibitor development in the active sites and in a conserved interdomain cavity.

## Introduction

Living systems provide nitrogen to their biosynthetic pathways via the amide side chain of glutamine. Glutamine amidotransferases are the ubiquitous and centrally important enzymes that transfer the amide nitrogen of glutamine to a variety of substrates. Each glutamine amidotransferase is a complex enzyme. Glutamine is hydrolyzed to ammonia and glutamate in a glutaminase domain or subunit. Labile ammonia is channeled through an internal tunnel to a second catalytic domain or subunit, where a specific acceptor substrate is subject to nucleophilic attack by ammonia [1]. Tunnels between physically separate active sites, catalytic coupling, and intramolecular signaling pathways are recurring features of glutamine amidotransferases [2–5]. Channeling of labile metabolic intermediates has been widely discussed and anticipated but has eluded direct experimental verification for all but intramolecular channels. Tryptophan synthase, which channels indole, is the paradigm for enzymes with internal channels [6]. Glutamine amidotransferases are the only other well-characterized systems where substrate loss, by diffusion or by competitive hydrolytic processes, is eliminated through direct transfer of an intermediate. Catalytic coupling in most glutamine amidotransferases occurs when catalysis in the glutaminase active site is initiated by substrate binding to the subsequent active site. This increases the success rate of the overall process by lowering the probability of uncoupled catalytic events. Interdomain signaling is required to couple catalysis in remote active sites and necessarily involves protein conformational change. The mechanisms of channeling and catalytic coupling appear to depend upon the structure of the individual enzyme. For example, both transient [3] and permanent [2, 4, 5] ammonia channels of varying polarity have been observed in glutamine amidotransferases. Each of these large, multidomain enzymes has several important conformations in its complex reaction cycle. Structures of all relevant states have not yet been obtained for any glutamine amidotransferase, and no common features in the mechanisms of channeling, catalytic coupling, and signaling have yet emerged.

Imidazole glycerophosphate synthase (IGPS) [7, 8] provides a new example of substrate channeling and interdomain signaling by glutamine amidotransferases. IGPS catalyzes the bifurcation step of the histidine and de novo purine biosynthetic pathways, converting $N^1$-(5′-phosphoribosyl)-formimino-5-aminoimidazole-4-carboxamide ribonucleotide (PRFAR) to imidazole glycerol phosphate (ImGP) and 5′-(5-aminoimidazole-4-carboxamide) ribonucleotide (AICAR) (Figure 1b). IGPS is a potential target for the development of antifungal, antibacterial, and herbicide agents because the histidine biosynthetic pathway does not occur in mammals. Two active sites may be exploited for this purpose. Ammonia generated by a glutaminase domain in the first step of the reaction is transferred to a cyclase domain where it acts as a nucleophile to react with PRFAR in the second reaction step [7, 8]. PRFAR is required to initiate the glutamine hydrolysis reaction. Crosstalk between the domains and ammonia channeling are postulated to explain the tight coupling of the two active sites. In bacteria, IGPS is formed by physical association of two poly-

[3] Correspondence: smithj@purdue.edu
[4] Present address: Laboratory of Structural Biology and Molecular Medicine, University of California, Los Angles, California 90095.
[5] Present address: Department of Biochemistry and Molecular Biology, Indiana University School of Medicine, Indianapolis, Indiana 46202.

**Key words:** ammonia tunnel; glutamine amidotransferase; histidine biosynthesis; intermediate channeling

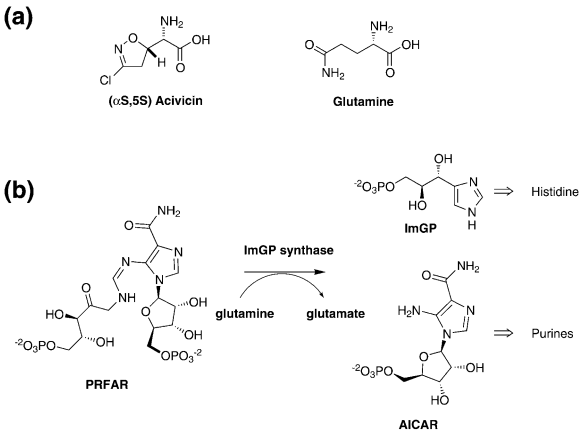


Figure 1. Schematic Diagram of IGPS Reactants and Products

(a) Substrate glutamine and analog acivicin.

(b) Chemical reaction catalyzed by the cyclase domain of IGPS.

peptides, the glutaminase (HisH) subunit and the cyclase (HisF) subunit [7]. In fungi and plants, the two domains are fused into a single, 60 kDa polypeptide with the glutaminase domain at the N terminus [9, 10].

The glutaminase domain of IGPS belongs to the triad family, one of at least three families among the glutamine amidotransferases [1]. Structures have been reported for three other members of the triad family: GMP synthetase (GMPS) [11], carbamoyl phosphate synthetase (CPS) [2], and anthranilate synthase (AS) [12]. The name "triad" refers to a conserved catalytic triad motif (Cys-His-Glu), which is organized similarly to the catalytic triad of cysteinyl proteases [11]. However, the triad amidotransferase fold is unique in the structural database, unrelated to other hydrolytic enzymes. Sequence identity is low among the triad amidotransferases (10%–25%) despite strong structural conservation.

The $NH_3$-acceptor site resides in the C-terminal domain of fungal IGPS. ImGP synthesis involves steps of $NH_3$-dependent C-N ligase, C-N lyase, and C-N cycloligase, the order and mechanism of which are not fully established [7, 13, 14]. The cyclase domain alone can catalyze ImGP production from $NH_3$ in the reaction medium, albeit less efficiently than in the glutamine-dependent reaction [7]. Recently the cyclase domain was shown to be a $(\beta/\alpha)_8$ barrel in the crystal structure of the HisF subunit of IGPS from the thermophilic bacterium *Thermotoga maritima* [15]. Sequence similarity and structural resemblance suggest an ancient gene duplication of half-barrels to form the whole barrel [15, 16].

Here, we present the 2.1 Å crystal structure of intact IGPS from *Saccharomyces cerevisiae*. The glutaminase domain is inactivated by acivicin (Figure 1a), a glutamine analog and a potent chemotheraputic agent [13]. The structure of IGPS shows an unprecedented use of the $(\beta/\alpha)_8$ barrel as an ammonia tunnel joining the glutaminase and cyclase active sites. Mechanisms of substrate channeling and interdomain signaling are discussed in the context of the intact enzyme structure.

## Results and Discussion

### Description of the Structure

IGPS is composed of two domains, an N-terminal glutaminase domain (residues 1–235) and a C-terminal cyclase domain (residues 239–552) (Figures 2 and 3). The prefixes "h" and "f" designate elements of secondary structure in the N- and C-terminal domains, respectively, with reference to the HisH and HisF subunits of bacterial IGPS. Although crystals of IGPS have two molecules in the asymmetric unit, the protein is a monomer in the crystal structure, consistent with experimental findings that IGPS is a monomer in solution [10]. The two molecules are essentially identical, having an rmsd of 0.25 Å for 533 equivalent Cα atoms.

The first three residues (Gly-3, Ser-2, and His-1), which remain after thrombin cleavage of polyhistidine-tagged IGPS, form a square-planar complex with $Ni^{+2}$. The planar $Ni^{+2}$ complex is part of a crystal lattice contact that also involves four to five interprotein hydrogen bonds. This structural feature explains why IGPS crystals could be grown only from thrombin-cleaved, His-tagged protein that had not been treated with metal chelators. The N-terminal pentapeptides (Gly-Ser-His-Met-Pro-) are oriented differently in the two independent IGPS molecules due to small differences in crystal packing.

### Glutaminase Domain and Its Active Site

The N-terminal glutaminase domain of IGPS is similar to other glutaminase domains of the triad amidotransferase family, namely GMPS, CPS, and AS (Table 1). The fold is built around a central, open, twisted, mostly parallel β sheet, flanked by α helices, β strands, and irregular loops (Figures 2 and 3). The active site is in a cleft on the C-terminal edge of the central β sheet and faces the domain interface. The catalytic triad (Cys83, His193, and Glu195) is at the ends of adjacent β strands in the central sheet (hβ4 and hβ11) and is arranged similarly to the Cys-His-Glu triads of GMPS, CPS, and AS (Figure 4). In IGPS, the Sγ atom of Cys83 is within hydrogen bonding distance of the imidazolium nitrogen of His193 and the carbonyl oxygen of Gly49 from the adjacent β strand (hβ3; Figure 5). As in the other triad amidotransferases, Cys83 occurs in a "nucleophile elbow" motif, marked by the fingerprint sequence -Gly-X-Cys-X-Gly-, and it has a backbone conformation in the forbidden region of the Ramachandran plot ($\phi = 58°$, $\psi = -110°$). In this respect, the triad amidotransferases are similar to the α/β hydrolases [17] although the overall topology and order of catalytic residues differ in the two protein families.

The glutaminase active site resides in an interdomain cavity that is inaccessible to bulk solvent in the crystal structure. The surface of this cavity is polar and lined with a number of conserved residues from both domains. The glutamine binding site is defined by electron density for a covalent adduct at nucleophilic Cys83 (Figure 4), the product of enzyme inactivation by the glutamine analog acivicin (Figure 1a). Positions of the α-$NH_3^+$ and α-$COO^-$ groups of the adduct are well defined by density and within hydrogen bonding distance of conserved residues in the cavity (Gly51, Gln87, Glu95, Ser148, Phe149, and Gln397; Figures 4–6). An important feature of glutamine specificity is the hydrogen bond to Gln397, which is in the cyclase domain and may contribute to the signal from substrate binding in the cyclase active site. Most of the contacts conferring glutamine specificity in IGPS are similar to those found in CPS. However, the orientation of the glutamine analog in the

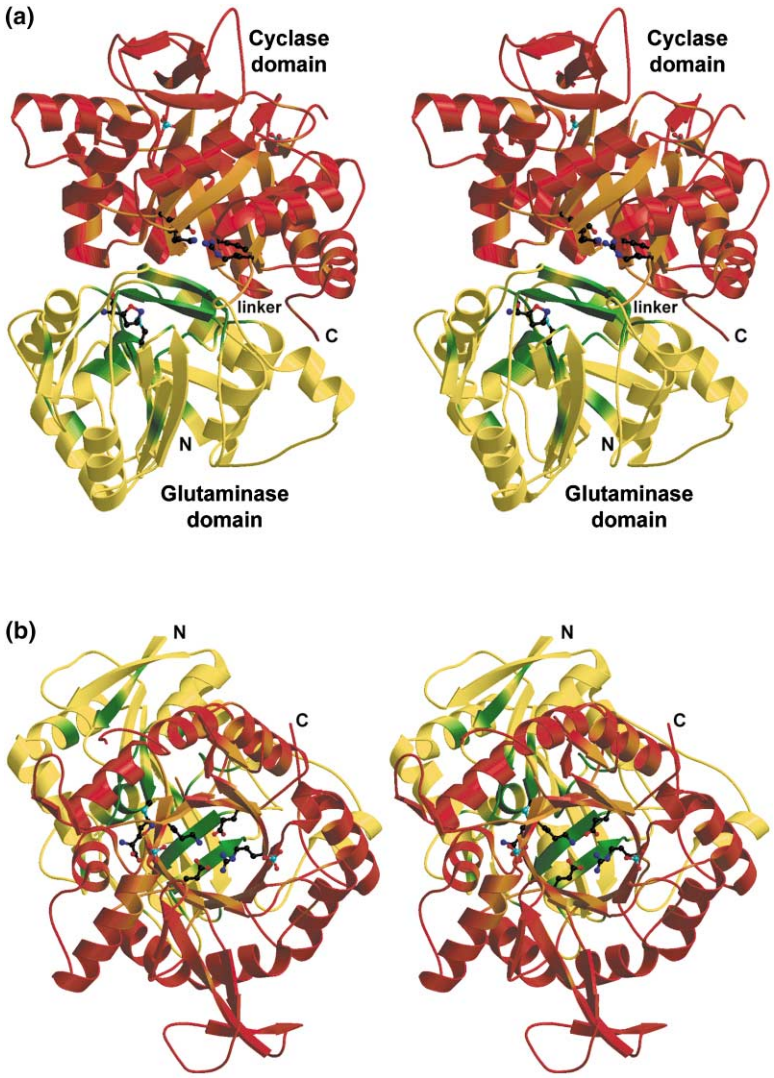


Figure 2. Structure of IGPS

The close association of the glutaminase (yellow) and cyclase (red) domains is apparent in the ribbon diagrams. Sites of sequence conservation are shaded green in the glutaminase domain and orange in the cyclase domain.

(a) Side view.

(b) View from the top of the $(\beta/\alpha)_8$ barrel of the cyclase domain, perpendicular to (a).

All atoms are drawn for the acivicin adduct at Cys83 in the glutaminase domain, for the two sulfate ions in the cyclase active site and for the 4 residue charge gate at the domain interface (C, black; O, red; N, blue; and S, cyan).

active site of IGPS differs from that of the glutamyl thioester and γ-semialdehyde complexes of CPS [18, 19]. As a result, the α-$NH_3^+$ and α-$COO^-$ groups of acivicin are farther from the hβ3 strand and closer to the hβ11 (His193) strand in IGPS than in CPS (Figure 5). Although electron density for the covalent adduct is not consistent with the expected structure of acivicin-inactivated Cys83 near the Sγ atom (Figures 1 and 4; [13]), important elements of glutamine specificity in the active site are revealed by the complex.

An "oxyanion hole," which stabilizes the negative charge during the hydrolytic reaction, is a recurring feature among enzymes with catalytic triads. In triad amidotransferases, two amide nitrogens comprise the canonical oxyanion hole, one from the residue immediately following the nucleophile (Val84) and the second from an adjacent β strand (residues 44–51, hβ3, henceforth referred to as "oxyanion strand") (Figure 5). The helix dipole beginning at Val84 (hα4) may also stabilize the oxyanion. In GMPS, CPS, and AS, the oxyanion strand includes the highly conserved sequence Ser48-Xaa49-Gly50 (IGPS numbering), in which the NH of Gly50 points into the catalytic site and is part of the oxyanion hole. The orientation of the peptide between residues 49 and 50 is enforced by a hydrogen bond between the Ser48 OH and the backbone C=O of residue 49 (Figure 5). In IGPS, Pro48-Gly49-Val50-Gly51 is one of the most conserved sequences, although Pro48 cannot form such a hydrogen bond. Instead, the C=O of Gly49 points into the active site in close contact with Cys83 Sγ, and no amide nitrogen in the oxyanion strand of IGPS is oriented toward the active site. We observed no electron density for either adduct or water in the presumed oxyanion hole of any IGPS crystal. The unexpected conformation of the oxyanion strand was confirmed in a simulated-annealing omit map [20] and was also shown not to result from the acivicin adduct at Cys83 (data not shown). Two possibilities may account for the observed conformation of the oxyanion strand. First, the oxyanion may be stabilized by interaction with only the NH of Val84 and the helix dipole. Alternatively, an oxyanion hole may form only when the glutaminase domain is activated by PRFAR binding to the cyclase domain. In this regard, a hydrogen bond between the NH of Asn52 at the end of the oxyanion strand and the C=O of Ala393 in the cyclase domain may be important (Figure 6).

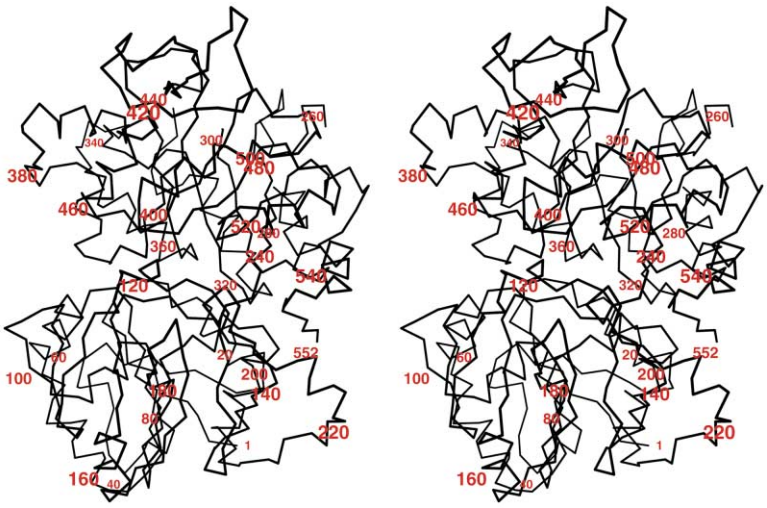


Figure 3. Cα trace of IGPS

The view in this stereo diagram is identical to Figure 2a.

The glutaminase active site as seen in the crystal structure may not be in a fully active state. IGPS has no glutaminase activity in the absence of the labile cyclase substrate PRFAR [10], which did not survive crystallization. A different position for the glutamine analog within the active site cavity of IGPS relative to CPS and the apparently unformed oxyanion hole suggest that activation leads to structural changes within the glutaminase domain that position glutamine appropriately for hydrolysis, while maintaining the elements of recognition. A dynamic glutamine active site is also consistent with the slightly different orientations of acivicin in the two independent molecules in IGPS crystals.

### The Cyclase Domain and Its Active Site

The C-terminal cyclase domain of yeast IGPS is a classic $(\beta/\alpha)_8$ barrel (Figure 2b). It is very similar to the HisF cyclase subunit of bacterial IGPS ([15]; Table 1); the most striking difference is the longer loops at the top of the yeast IGPS barrel (Figure 7). The first five of these β-loop-α connections are 3–19 residues longer in the yeast domain than in the bacterial subunit, accounting for nearly all of the 60 additional residues of the yeast domain. The insertions, which are characteristic of fungal IGPS sequences, occur at the exterior of the barrel away from the active site, for the most part in regions of low conservation. Conserved residues in the loops occur toward the active site, nearer the center of the barrel and the β strands (Figures 2a and 2b). Long β/α loops sequester the active site in certain $(\beta/\alpha)_8$ barrel enzymes, e.g., pyridoxine phosphate synthase [21] and indole glycerol phosphate synthase [22], and may also sequester PRFAR and the cyclase active site in IGPS. However, such interactions are unlikely to be specific due to the lack of conserved residues in these loops.

In contrast to the long β-loop-α connections at the top of the barrel, the α-loop-β connections at the bottom of the barrel are conserved, short, and identical to those in the bacterial subunit. The N- and C-terminal peptides of the yeast and bacterial cyclase domains are remarkably similar, given the lack of a glutaminase subunit in the bacterial cyclase structure. Like the bacterial subunit, the yeast cyclase domain exhibits internal pseudosymmetry. (Ninety pairs of Cα atoms in the $(\beta/\alpha)_4$ halves of the barrel superimpose with an rmsd of 1.7 Å and have 17% sequence identity.) However, the insertions in the first five β-loop-α connections effectively limit the internal pseudosymmetry to the core and bottom of the barrel of yeast IGPS.

The top of $(\beta/\alpha)_8$ barrel enzymes is a common active "supersite" [23] and was assigned as the cyclase active site of the bacterial HisF subunit [15] based on the positions of two bound phosphate ions that mimic the two phosphate groups at the ends of PRFAR (Figure 1). Sul-

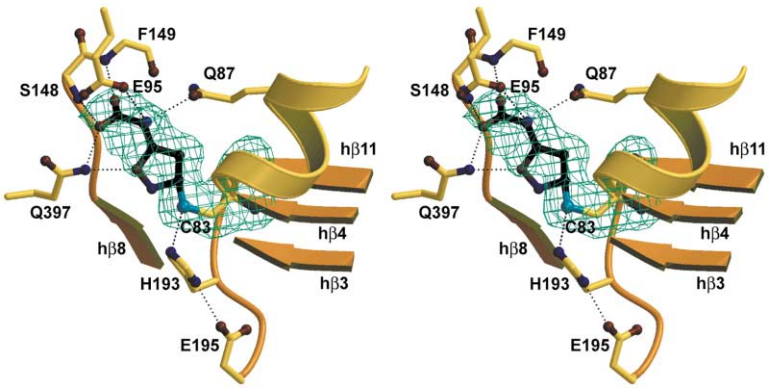


Figure 4. Glutaminase Active Site with Acivicin Adduct at Cys83

Protein groups participating in polar interactions with the bound acivicin in one molecule of IGPS are shown in stereo. Electron density at 2.1 Å resolution is contoured in cyan at three times the rms level of the map. The map was computed with $\sigma_A$-weighted phases from the final model, omitting atoms for acivicin and Cys83. The catalytic triad (Cys83-His193-Glu197) is shown. Atom coloring is as in Figure 2.

Table 1. Structure Alignment of IGPS Domains with Homologous Proteins

| Molecule | Rmsd (Å) | Number of Cα Atoms/ Number Aligned | Structure-Based Sequence Identity (%)[a] | PDB code [ref] |
|---|---|---|---|---|
| Glutaminase domain | | | | |
| GMPS | 1.9 | 206/142 | 20 | 1GPM [11] |
| CPS | 1.9 | 225/134 | 17 | 1A9X [2] |
| AS | 1.8 | 195/133 | 24 | 1QDL [12] |
| Cyclase domain | | | | |
| HisF | 1.6 | 306/233 | 46 | 1THF [15] |
| HisA | 1.8 | 241/186 | 20 | 1QO2 [15] |

[a] Calculated as number of identical aligned residues/number of aligned residues

fate ions occupy similar sites in yeast IGPS, which was cocrystallized with labile PRFAR and ammonium sulfate. As expected, no electron density was observed for PRFAR, which would fit comfortably between the sulfate/phosphate sites. The PRFAR binding site in IGPS forms a trench across the top of the cyclase barrel and is lined with many conserved residues, several of which are essential to catalysis ([14]; Figures 2a and 2b).

The internal pseudosymmetry of the cyclase domain is exploited in binding the PRFAR phosphate groups. The sulfate/phosphate ions occupy pockets on opposite sides of the barrel top, one between loops fβ/α3 and fβ/α4 and one between loops fβ/α7 and fβ/α8 (Figure 7). The pseudosymmetric loops fβ/α4 and fβ/α8 have helical insertions, fα4′ and fα8′, with the bound ions hydrogen bonded to peptide NHs at the N termini of both helices. This is a common phosphate-specificity motif found between fβ/α7 and fβ/α8 of several other $(\beta/\alpha)_8$ barrel enzymes [23–25].

Some features of ion binding to the cyclase domain of yeast IGPS suggest that it mimics the binding of PRFAR phosphates in an initial substrate complex. First, the ions in both phosphate sites are bound to the protein through water-bridged hydrogen bonds. Second, at the site between fβ/α7 and fβ/α8, two phosphate subsites have been identified in the two independent molecules of yeast IGPS and in the bacterial cyclase structure. Both the variability in ligand binding and the solvation of bound ions are consistent with an initial, precatalytic complex. Conformational changes upon PRFAR binding may draw the substrate further into the enzyme, desolvating the phosphate groups and binding them in specific sites.

## Organization of the Intact Enzyme

The catalytic domains of IGPS are arranged to channel $NH_3$ from the glutaminase active site to the cyclase active site. Remarkably, the glutaminase active site points directly into the bottom of the cyclase $(\beta/\alpha)_8$ barrel, with the conserved barrel interior serving as the $NH_3$ tunnel (Figures 2a and 8). The tunnel is blocked by a "gate" of four buried and charged amino acids at the bottom of the barrel. Below the gate, a polar chamber (chamber I) at the domain interface leads to the glutaminase active site. Above the gate, a hydrophobic tunnel (chamber II) leads to the cyclase active site. The barrel passageway is an entirely new organization for an amidotransferase $NH_3$ tunnel.

### *The $NH_3$ Freeway: Chamber I*

Chamber I connects the $NH_3$-generation site to the base of the barrel and is between the catalytic domains. The glutaminese active site cavity is oriented to release $NH_3$ directly into chamber I (Figure 8). This part of the $NH_3$ passage is quite polar and formed mainly by residues on loops near the glutaminase active site. Chamber I is lined with conserved residues and, along with the two active sites, may be a site for targeted drug or herbicide design.

### *The Domain Interface*

The domain interface is among the most conserved regions of IGPS (Figure 2a). The extensive interface buries approximately 1700 Å$^2$ of surface area from the two do-

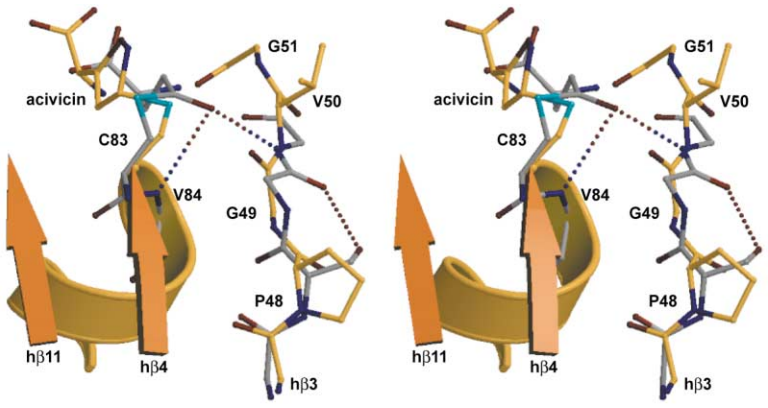


Figure 5. Oxyanion Hole in IGPS and Carbamoyl Phosphate Synthetase

The oxyanion hole of the IGPS glutaminase active site (yellow, as the acivicin complex) with superimposed segments of CPS (gray, as the glutamate thioester complex) is shown in stereo. Two hydrogen bonds (dotted lines) in the CPS complex form the oxyanion hole, which is stabilized by a third hydrogen bond between Ser $O_\gamma$ and C=O of the following residue in the conserved Ser-Xaa-Gly motif. GMPS and AS are like CPS in sequence and conformation. The glutamine analog in IGPS is far from the oxyanion hole, relative to the CPS complex, due to a 150° difference in rotation of the Cys83 Cβ-Sγ bond. Atom coloring is as in Figure 2.

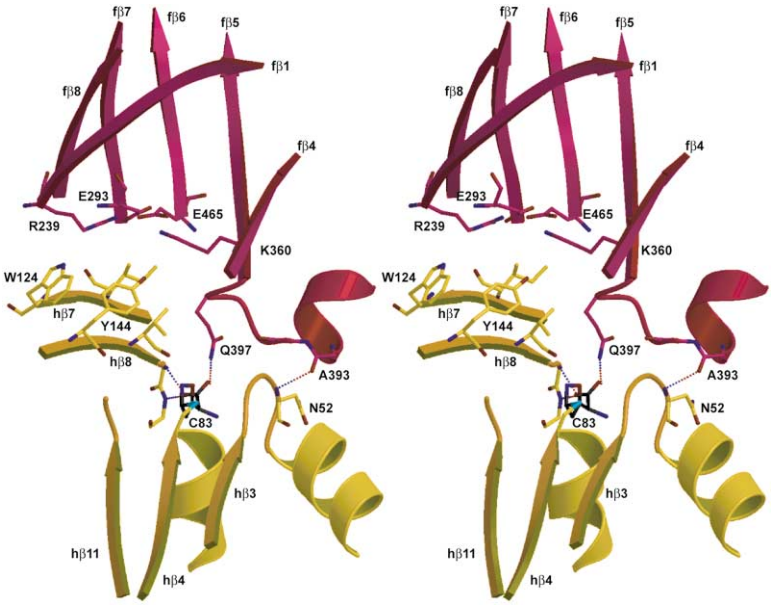


Figure 6. Intimate Connection between the Cyclase Domain and the Glutamine Active Site

Structure elements are shown in yellow for the glutaminase domain and in magenta for the cyclase domain in this stereo diagram. Hydrogen bonds are drawn as dotted lines.

mains (Figure 9). The contacting surfaces are largely polar except for a hydrophobic patch formed by the hβ7-hβ8 sheet, which packs against Pro and Gly residues at the bottom of fβ3, fβ6, and fβ7 (Figure 6). Most of the 14 hydrogen bonds between domains involve α-loop-β connections following helices fα2, fα3, and fα4 at the bottom of the cyclase barrel. Many more contacts are mediated by 18 water molecules buried in the domain interface. Two of the three backbone hydrogen bonds between domains may affect catalytic regions of the glutaminase domain: NH of Asn52 in the oxyanion strand (residues 44–51) to Ala393 C=O, and NH of Gly198 near the catalytic triad (His193 and Glu195) to Phe324 C=O. Two α helices in the cyclase barrel are oriented for favorable dipolar interactions with helices in the glutaminase domain: fα3 with hα1 and fα4 with hα2. The Asn52-Ala393 hydrogen bond is part of the latter dipolar interaction (Figure 6).

The peptide linking the catalytic domains of IGPS is highly conserved (Leu236-Thr/Ala237-Arg/Lys238) and makes several hydrophobic contacts and hydrogen bonds with both domains. Likewise, conserved residues in the adjacent C-terminal peptide interact specifically with both domains. Hydrogen bonds and hydrophobic interactions link conserved residues Trp124 from the glutaminase domain, Thr237 NH of the linker peptide, Arg548 from the C-terminal peptide, and Asp292 adjacent to the gate. Thus, conformational changes in this region of the structure are likely to be highly coupled and may lead to restructuring of the domain interface.

### *A Closed Gate at the Bottom of the Barrel*

Four conserved and charged residues in the cyclase domain form a network of buried salt links at the bottom of the barrel (Figures 6 and 8). Arg239, Glu293, Lys360, and Glu465 are contributed by the N termini of strands fβ1, fβ3, fβ4, and fβ6, respectively. These residues create a barrier to $NH_3$ (radius ~1.4 Å). We call this network a "charge gate" in the $NH_3$ passageway.

### *The $NH_3$ Freeway: Chamber II*

Chamber II of the proposed $NH_3$ channel is hydrophobic and is formed by four layers of inward-pointing side chains on the β strands of the $(\beta/\alpha)_8$ barrel (Figure 8). The first layer is formed by the invariant residues of the charge gate. The surface of chamber II is formed by small, aliphatic side chains that are conserved in size and character (Ile241, Thr328, Val400, Ile497, and Ala519 in layer two and Thr295, Ser362, Leu467, and Leu521 in layer three). The few polar side chains in these layers

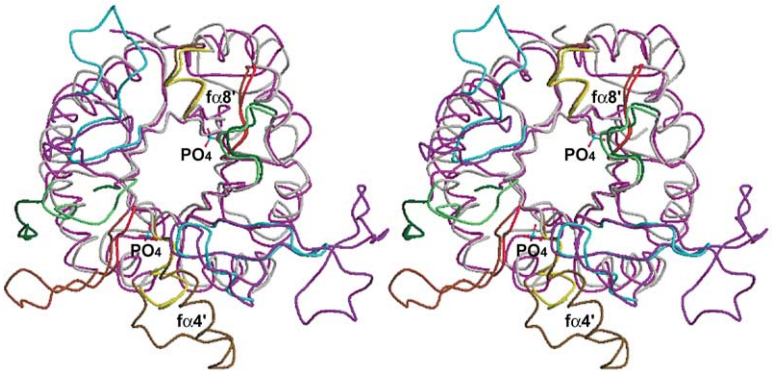


Figure 7. Comparison of Fungal and Bacterial Cyclase Domains

The superposition of 233 Cα atoms in the $(\beta/\alpha)_8$ cyclase domains of yeast (magenta) and *T. maritima* [15] (gray) IGPS is shown as a stereo Cα trace. Loops at the top of the barrel are colored according to pseudosymmetry (βα1 and βα5 are blue, βα2 and βα4 are green, βα3 and βα7 are red, and βα4 and βα8 are yellow), with loops from yeast IGPS in darker colors. In IGPS, 14 residues are missing from βα1 and four residues from βα2. The internal pseudosymmetry in length and conformation of these loops in bacterial IGPS is not observed in fungal IGPS.

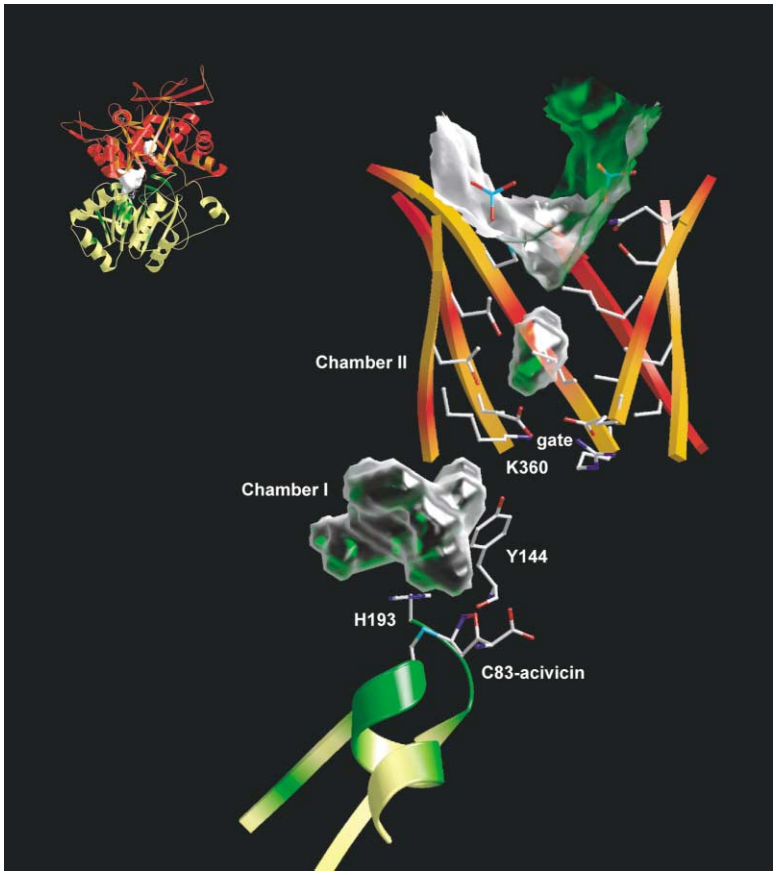


Figure 8. Channeling Pathway between Active Sites in IGPS

From bottom to top, the diagram shows atomic details for Cys83, acivicin, His193, and Tyr144 in the glutaminase domain, and the charge gate, three upper layers of side chains forming the hydrophobic tunnel, and sulfate ions in the cyclase domain. Surfaces are shown for polar chamber I at the domain interface, hydrophobic chamber II inside the $(\beta/\alpha)_8$ barrel, and the PRFAR binding site at the top of the barrel. Elements of secondary structure are colored as in Figure 2. The inset shows the positions of chambers I and II in the complete polypeptide.

form hydrogen bonds with gate residues and with buried water. The leucine side chains in layer three constrict the $NH_3$ tunnel and close the top of chamber II (Figure 8). Side chains in the fourth layer (Cys243, Leu297, Gly330, Gly364, Ser402, Asn469, Ser499, and Ala523) are more polar and form the base of the PRFAR binding site.

***The $(\beta/\alpha)_8$ Barrel as a Total Catalytic Domain***

The $(\beta/\alpha)_8$ "TIM" barrel is one of the most abundant folds in the structural database, forming at least 18 homologous families with immense catalytic versatility and sequence variability. The top of the barrel is the catalytic site in the generic $(\beta/\alpha)_8$ enzyme, IGPS being no exception. However, IGPS is unique among $(\beta/\alpha)_8$ enzymes in its complete functional utilization of the barrel architecture, which is well suited to the complex multicatalytic tasks of this enzyme. The cyclase active site is at the top of the barrel. At the bottom of the barrel, Gln397 contributes to substrate specificity in the glutaminase active site. The bottom of the barrel also houses the charge gate to the $NH_3$ passageway, physically separating the two IGPS active sites. Most dramatically, the interior of the barrel channels $NH_3$ to the cyclase active site. Channeling is a rare function for the $(\beta/\alpha)_8$ barrel, which in most cases is filled with large, hydrophobic side chains. Open-barrel proteins have small side chains inside the barrel; their backbone conformation does not distinguish them from closed-barrel proteins. Other examples of open barrels include a polar water channel in pyridoxine 5′-phosphate synthase [21] and a binding site for CoA in methylmalonyl CoA mutase [26]. The gated $NH_3$ tunnel in IGPS is an adaptation of this ubiquitous protein fold for even more sophisticated biological function.

**Catalytic Coupling**

The structure of intact IGPS shows how the glutaminase and cyclase catalytic modules are assembled and function together in this complex enzyme. The glutaminase domain generates $NH_3$ in an enclosed polar chamber at the domain interface. Its escape from the enzyme thus prevented, $NH_3$ passes through a hydrophobic tunnel in the center of the $(\beta/\alpha)_8$ barrel to reach PRFAR in the cyclase active site.

The structure also provides a framework for studying the mechanism of catalytic coupling of the physically separate active sites. The stoichiometry of the overall reaction is controlled in IGPS, as in most other glutamine amidotransferases [1], by disabling the glutaminase when the $NH_3$-acceptor substrate (PRFAR) is not present [7, 13]. Thus, at least two enzyme conformations exist in the IGPS catalytic cycle: a PRFAR-present state having an active glutaminase and a PRFAR-absent state having no glutaminase activity. Several factors indicate that the crystal structure represents a PRFAR-absent conformation of the enzyme. PRFAR is not present. The glutaminase active site is inaccessible to molecules in the bulk solvent. The glutaminase oxyanion hole appears to be incomplete. The charge gate blocks the path between the glutaminase and cyclase active sites. Finally, the yeast cyclase domain and the bacterial cy-

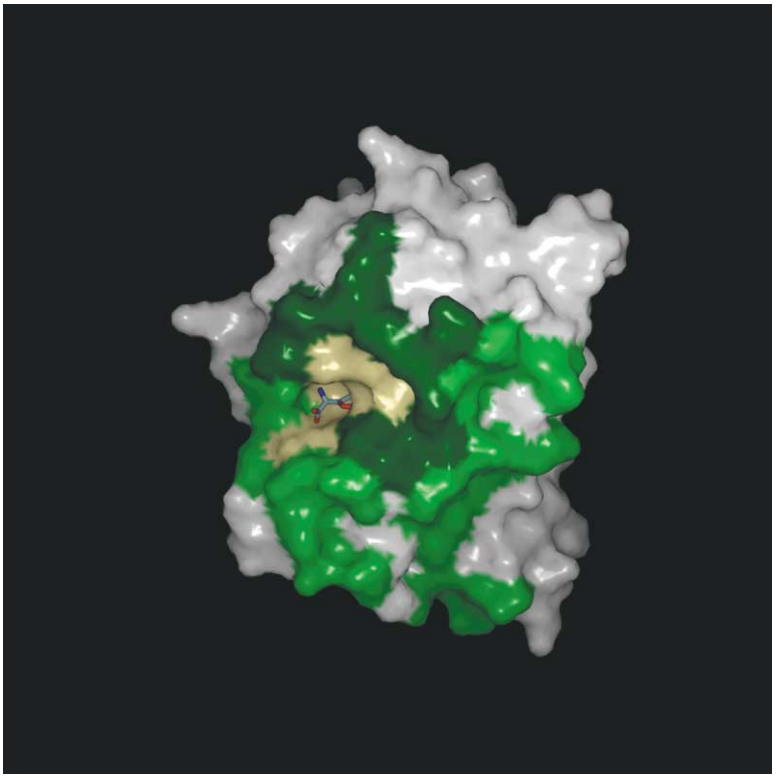

Figure 9. Surface of the Interface Region of the Glutaminase Domain

The glutamine analog bound to Cys83 protrudes from a concavity on the surface of the domain. The footprint of the cyclase domain is green, with a darker shade for residues also contributing to the polar chamber. Other surfaces of the polar chamber and glutaminase active site cavity are yellow.

clase subunit, also lacking PRFAR, are remarkably alike in the region between the active site and the interface with the glutaminase domain. Thus, we interpret the crystal structure as a "presignaling" form of IGPS.

The simplest way for PRFAR binding at the top of the cyclase barrel to activate the glutaminase domain at the bottom is through changes in the extensive domain interface. Several specific interactions link the glutaminase active site directly to the domain interface, so that modest conformational changes in the cyclase domain may have a large effect on the glutaminase active site (Figure 6). For example, Gln397 in the cyclase domain contacts the glutaminase substrate. The hβ7-hβ8 β ribbon of the glutaminase domain has extensive hydrophobic contacts with the cyclase domain and connects directly to the glutamine substrate through the backbone hydrogen bonds of Ser148 and Phe149 (Figure 4). The glutaminase oxyanion strand is linked to the cyclase domain by a backbone hydrogen bond from Asn52 to Ala393. Several experimental results show that the domain interface is critical to IGPS function. Residues in the interface are highly conserved among IGPS sequences. Mutagenesis of the domain interface region of the *E. coli* IGPS cyclase subunit affected glutaminase activity in the holoenzyme [8]. Engineered N- and C-terminal half-barrels of the *T. maritima* cyclase subunit formed a heterodimer that associated readily with the glutaminase subunit but had no glutamine-dependent catalytic activity [27].

We propose that PRFAR binding to the top of the cyclase barrel induces conformational changes in the glutaminase interface at the bottom, transmitted either through the side chains of β strands in the barrel interior or through the exterior α helices. No specific path of conformational change is apparent from the structure or other data, although likely candidates abound. For example, the network of contacts involving the linker and C-terminal peptides indicate that these regions of the cyclase domain, which are outside the barrel framework, are primed to transmit conformational change. Similarly, the 18 buried waters at the domain interface may act as molecular lubricants and assist in structural reorganization of the interface. Changes in the domain interface are predicted to have at least two effects on the glutaminase active site. The oxyanion strand will rearrange to contribute the backbone NH of either Gly49 or Val50 to an oxyanion hole as in the substrate complexes of CPS (Figure 5). In addition, glutamine-specificity elements (Gln397 and the hβ7-hβ8 β ribbon) will move closer to the catalytic triad and oxyanion hole so that when glutamine is bound, its amide is adjacent to Cys83 with the carbonyl oxygen in the oxyanion hole.

Another important result of signaling between the catalytic domains must be the opening of the buried charge gate to admit $NH_3$ to the hydrophobic tunnel and the cyclase active site at the top of the barrel. The strength of a salt link in a protein is specific to its environment, being especially strong when buried in a hydrophobic environment such as the charge gate in the interior of IGPS. The need to maintain zero net charge in this environment and to sequester $NH_3$ argues against major reorganization of the charge gate. We note that rotation of the Lys360 side chain to form a hydrogen bond with the hydroxyl of Tyr144 would open the gate enough for $NH_3$ to pass while retaining electrostatic contact with the charge gate (Figure 6). Invariant Tyr144 is part of

Table 2. Crystallographic Summary

| | SeMet IGPS | | | Wild-Type IGPS |
|---|---|---|---|---|
| **Diffraction data** | | | | |
| Beamline | | 14BM-D BioCARS | | 17ID IMCA |
| Detector | | ADSC Q4 | | MAR CCD |
| Unit cell (Å) a, b, c ($P2_12_12_1$) | | 99.0,112.2, 116.2 | | 99.4, 112.2 116.7 |
| λ (Å) | 0.9796 | 0.9795 | 0.9537 | 1.000 |
| Data range (Å)[a] | 100–2.4 (2.49–2.4) | 100–2.4 (2.49–2.4) | 100–2.4 (2.49–2.4) | 100–2.1 (2.18–2.1) |
| $R_{merge}$[b] | 0.051 (0.24) | 0.043 (0.20) | 0.053 (0.25) | 0.067 (0.39) |
| Average multiplicity | 7.3 (7.3) | 5.9 (5.9) | 5.0 (5.0) | 14.3 (13.1) |
| Completeness (%) | 99.2 (95.1) | 98.1 (93.6) | 99.2 (96.3) | 100 (99.9) |
| Average I/σ | 7.9 (3.1) | 7.9 (3.4) | 8.0 (3.2) | 7.3 (2.0) |
| **Model refinement** | | | | |
| Resolution range | | | | 50–2.1 Å |
| Number of reflections ($I/\sigma_I > 0$) | | | | 75,906 |
| Number of atoms | | | | 8,801 |
| R factor[c] | | | | 22.2% |
| $R_{free}$[c] | | | | 24.2% |
| Rmsd bond length | | | | 0.008 Å |
| Rmsd bond angle | | | | 1.4° |
| Average B (protein) | | | | 30.7 Å$^2$ |
| Average B (water) | | | | 33.3 Å$^2$ |
| Average B (ligand) | | | | 57.4 Å$^2$ |
| Rms ΔB (bonded atoms) | | | | 1.2 Å$^2$ |
| Estimated coordinate error | | | | 0.24 Å |

[a] Numbers in parentheses correspond to data in the outermost resolution shell.
[b] $R_{merge} = \Sigma_h\Sigma_i|I_{h,i} - <I_h>|\Sigma_h\Sigma_i I_{h,i}$
[c] R factor $= \Sigma||F_{obs}| - |F_{calc}||/\Sigma|F_{obs}|$; $R_{free}$ for a 5% subset of reflections.

the hβ7-hβ8 contact surface of the glutaminase domain. The net neutrality of the buried charge gate also may prevent $NH_3$ from acquiring a proton as it passes through the gate. Similarly, hydrophobic chamber II above the gate should be an effective ion filter to keep unreactive $NH_4^+$ or undesired charged nucleophiles, especially $OH^-$, away from PRFAR.

The crystal structure places onstage the three main players in the catalytic drama of IGPS—the glutaminase active site, the gated $NH_3$ channel, and the cyclase active site. It remains to see them in action.

## Biological Implications

Nitrogen is provided to biosynthetic pathways as the amide of glutamine. This fine control of nitrogen availability requires complex enzyme systems at biosynthetic steps of nitrogen addition. Glutamine amidotransferases are modular enzymes that hydrolyze glutamine in a glutaminase domain and deliver ammonia through an internal tunnel to an acceptor substrate in a second catalytic domain. Key features in the function of this important group of enzymes are the channeling mechanisms and signaling pathways used by each enzyme to couple the activities of physically separate active sites. The crystal structure of imidazole glycerol phosphate synthase, an amidotransferase of histidine biosynthesis, reveals new mechanisms to channel ammonia and to control glutaminase activity from the remote active site in a cyclase domain. The cyclase domain has the ubiquitous $(\beta/\alpha)_8$ barrel fold, with the glutaminase domain docked at the bottom of the $(\beta/\alpha)_8$ barrel. Ammonia is channeled through the interior of the barrel to the cyclase active site at the top. A gate of four conserved, charged amino acids in the cyclase domain controls access to the ammonia tunnel. Thus, all elements of the barrel architecture contribute to enzyme function, an unprecendented observation. Substrate binding to the cyclase active site controls glutaminase activity, in part by glutamine binding in a nonproductive orientation in absence of the cyclase substrate. A large number of contacts between the bottom of the cyclase domain and the glutaminase active site, including direct contacts with the glutamine substrate, are situated to reorganize the glutaminase active site upon a signal from the cyclase active site. Several possibilities for design of inhibitors are presented in the two active sites of the enzyme and in an enclosed, conserved cavity at the domain interface.

## Experimental Procedures

### Protein Production, Purification, and Crystallization

Expression of *S. cerevisiae HIS7* by *E. coli* BL21(DE3)/p*HIS7-T7* [10] was induced by addition of 0.1 mM IPTG, and the culture was grown to $OD_{600}$ of 4.0 before harvesting by centrifugation at 1500 × g for 20 min at 4°C. Cell pellets from 4 l cell culture were resuspended in 80 ml 10 mM PIPES (pH 7.0) and lysed by ultrasonication with 10–30 s bursts followed by 30 s rests on ice. Then, the pellets were centrifuged at 12,000 × g for 20 min at 4°C. The supernatant was treated with 1% streptomycin sulfate and stirred for 10 min at 4°C, centrifuged at 12,000 × g for 20 min at 4°C, and loaded onto a His-Bind column charged with 50 mM $NiSO_4$ and equilibrated in binding buffer (20 mM Tris HCl, 5 mM imidazole, and 0.5 M NaCl [pH 7.9]). After a 16 column-volume wash with binding buffer, His7-tag was

eluted with 4.5 column volumes of elute buffer (20 mM Tris HCl, 200 mM imidazole, and 0.5 M NaCl [pH 7.9]). Active fractions (>3.0 U/mg) were pooled and vacuum dialyzed to 10% volume in 24 hr in 10 mM PIPES (pH 7.0). The concentrated protein solution was diluted to 1 mg/ml with cleavage buffer (20 mM Tris HCl, 150 mM KCl, and 2.5 mM $CaCl_2$ [pH 8.4]) and incubated with 20 U of thrombin at 25°C with constant shaking at 200 rpm for 7.5 hr. The cleavage reaction was passed through the His-Bind column and thrombin-cleaved His7 was recovered within 1.5 column volumes. The active fractions (>5.0 U/mg) were pooled and concentrated to 25 mg/ml by vacuum dialysis as above and stored at −80°C as beads formed by snap-freeze in liquid nitrogen. The yield of IGPS was 10 mg/l cell culture. SeMet IGPS was produced by expression of *HIS7* in the *E. coli* methionine auxotroph B834(DE3)/*pHIS7-T7* and was purified by using the same protocol as for the wild-type. IGPS activity was assayed by established methods [10].

A 10 mg/ml solution of wild-type IGPS was incubated for 30 min at room temperature in a 1:1:1 molar ratio with the substrate PRFAR and the substrate analog acivicin. The reaction mixture was used directly for crystallization at 20°C by hanging-drop vapor diffusion from a 1:1 mixture of protein solution and reservoir solution [22%–28% PEG MME 5000, 0.1 M MES (pH 6.5–7.0), and 0.2 M $(NH_4)_2SO_4$]. Crystals grew in 7–10 days to an average size of 120 × 120 × 80 μm. The crystals were washed in reservoir solution, cryoprotected by a quick dunk in reservoir solution plus 17%–29% ethylene glycol, and flash frozen in a nitrogen stream at 100 K. SeMet IGPS was also prereacted with PRFAR and acivicin, starting from an 8 mg/ml protein solution and with addition of 5 mM DTT after the 30 min incubation. Crystals were grown under the same conditions used for wild-type IGPS except that droplets were microseeded with wild-type IGPS crystals. SeMet IGPS crystals grew to 200 × 200 × 60 μm in 7–10 days and were cryoprotected in the same manner as wild-type IGPS crystals except for the addition of fresh 5 mM DTT to the washing and cryoprotectant solutions.

### Data Collection and Structure Determination

All diffraction data were recorded at the Advanced Photon Source (APS), Argonne National Laboratory. Three wavelength SeMet MAD data sets were collected at beamlines 14-BMD (BioCARS) and 17-ID (IMCA). Native data from a wild-type IGPS crystal of the same form were collected at 17-ID (IMCA). All data were processed and scaled with the HKL package [28]. Data quality is summarized in Table 2.

The structure was solved by MAD methods, by using the anomalous scattering of Se in SeMet-substituted protein. The low abundance of six Met residues in 555 amino acids produced a weak MAD signal, ~3% of |F|. The primitive orthorhombic unit cell has an asymmetric unit consisting of two IGPS molecules and ~43% solvent. All 12 Se sites were located by the Patterson-solving algorithm of the program SOLVE [29], which was also used to refine the Se partial structure and to compute phase probabilities. The initial 2.4 Å electron density map (average figure of merit 0.53) was clearly interpretable after solvent flattening and 2-fold averaging with DM [30]. A nearly complete atomic model of IGPS was built into the 2.4 Å map by using the graphics package O [31]. Model building was aided by reference to the structures of homologs: GMPS [11] (1GPM) for the N-terminal glutaminase domain of IGPS and *T. maritima* HisF [15] (1THF) for the C-terminal cyclase domain.

### Model Refinement

The initial model, including 530 residues in each of two IGPS molecules, was subjected to several cycles of reciprocal-space refinement interspersed with manual rebuilding. Refinement was done in the program CNS [32] by using all observations ($I/\sigma_I > 0$) in a 2.4 Å data set merged over all three wavelengths in the BioCARS MAD data. The resolution was extended to 2.1 Å with data from wild-type IGPS crystals. Two exposed loops in the C-terminal cyclase domain (residues 261–275 and 301–304) are disordered and were not modeled.

Ligands and water molecules were added to the model by using standard criteria. A $Ni^{+2}$ ion forms a square planar complex with the first three residues of the protein, preceding Met1. $Ni^{+2}$ ligands are the Nε atom of the His-1 side chain and the deprotonated backbone nitrogens of Gly-3, Ser-2, and His-1, causing both Ser-2 and His-1 to be Ramachandran outliers. No stereochemical restraints were applied to the $Ni^{+2}$ ion apart from a positional harmonic restraint. Ni was also detected by X-ray fluorescence (8.3 keV) from crystals used for MAD data collection at BM-14D and by color change upon addition of DTT to solutions of SeMet IGPS. Similar $Ni^{+2}$ complexes have not been reported in other protein structures, although the N-terminal His-tagged construct is commonly employed for protein production and the small-molecule structural database contains several square-planar, peptide-like complexes of $Ni^{+2}$ [33].

The glutaminase catalytic residue, Cys83, is modified by a covalent adduct, resulting from inactivation by acivicin, a glutamine analog. The electron density was not consistent with the expected product of acivicin inactivation, in which Cys Sγ displaces Cl (Figure 1) [13]. For all the data sets we examined, no density was visible at the expected N position in the 5 member ring, nor did any density support $sp^2$ geometry at the adduct C atom bonded to Sγ (Figure 4). Accordingly, an adduct model was built based on the results of a few iterations of dummy-atom addition at positions of maxima in $\sigma_A$-weighted $|F_o| - |F_c|$ electron density and automated refinement. An N atom was added to close the ring, in agreement with mass spectroscopic analysis of acivicin-inactivated enzyme [13]. A dictionary for the saturated acivicin adduct, based on similar substructures from the Cambridge database, was generated with XPLO2D [34] and modified manually. The true structure of the adduct could be masked by density that is an average of multiple adduct conformations, or, more likely, the density could correspond to a breakdown product of acivicin inactivation, formed during two weeks of crystal growth at 20°C.

The final model includes two polypeptide chains with a total of 1096 residues, 400 waters, 6 $SO_4^-$, 2 $Ni^{+2}$, and two Cys83 adducts (Table 2). Of the amino acids, 91.2% are in the core region of the Ramachandran plot [35]. Three residues per protein molecule are in disallowed regions but are supported by good electron density.

NACCESS [36], GRASP [37], CLUSTAL [38], VOIDOO [39], and programs from the CCP4 suite [30] were used for structure analysis. Model stereochemistry was checked with WHATIF [40] and PROCHECK [35]. Initial assignment of secondary structures was done with DSSP [41]. Figures were made with DINO (http://www.bioz.unibas.ch/~xray/dino), MOLSCRIPT [42], BOBSCRIPT [43], POV-ray (http://www.povray.org/), and Raster3D [44].

### Acknowledgments

This work was supported by National Institutes of Health grants DK42303 and GM24268 to J.L.S. and GM45756 to V.J.D. B.N.C. thanks A.K. Bera for helpful discussions.

Received: July 9, 2001
Revised: August 31, 2001
Accepted: September 6, 2001

### References

1. Zalkin, H., and Smith, J.L. (1998). Enzymes utilizing glutamine as an amide donor. Adv. Enzymol. Relat. Areas Mol. Biol. *72*, 87–144.
2. Thoden, J.B., Holden, H.M., Wesenberg, G., Raushel, F.M., and Rayment, I. (1997). Structure of carbamoyl phosphate synthetase: a journey of 96 Å from substrate to product. Biochemistry *36*, 6305–6316.
3. Krahn, J.M., Kim, J.H., Burns, M.R., Parry, R.J., Zalkin, H., and Smith, J.L. (1997). Coupled formation of an amidotransferase interdomain ammonia channel and a phosphoribosyltransferase active site. Biochemistry *36*, 11061–11068.
4. Binda, C., et al., and Mattevi, A. (2000). Crosstalk and ammonia channeling between active centers in the unexpected domain arrangement of glutamate synthase. Structure Fold. Des. *8*, 1299–1308.
5. Larson, T.M., et al., and Rayment, I. (1999). Three-dimensional structure of Escherichia coli asparagine synthetase B: a short journey from substrate to product. Biochemistry *38*, 16146–16157.

6. Miles, E.W., Rhee, S., and Davies, D.R. (1999). The molecular basis of substrate channeling. J. Biol. Chem. *274*, 12193–12196.
7. Klem, T.J., and Davisson, V.J. (1993). Imidazole glycerol phosphate synthase: the glutamine amidotransferase in histidine biosynthesis. Biochemistry *32*, 5177–5186.
8. Klem, T.J., Chen, Y., and Davisson, V.J. (2001). Subunit interactions and glutamine utilization by Escherichia coli imidazole glycerol phosphate synthase. J. Bacteriol. *183*, 989–996.
9. Kuenzler, M., Balmelli, T., Egli, C.M., Paravicini, G., and Braus, G.H. (1993). Cloning, primary structure, and regulation of the *HIS7* gene encoding a bifunctional glutamine amidotransferase:cyclase from *Saccharomyces cerevisiae*. J. Bacteriol. *175*, 5548–5558.
10. Chittur, S.V., Chen, Y., and Davisson, V.J. (2000). Expression and purification of imidazole glycerol phosphate synthase from *Saccharomyces cerevisiae*. Protein Expr. Purif. *18*, 366–377.
11. Tesmer, J.J., Klem, T.J., Deras, M.L., Davisson, V.J., and Smith, J.L. (1996). The crystal structure of GMP synthetase reveals a novel catalytic triad and is a structural paradigm for two enzyme families. Nat. Struct. Biol. *3*, 74–86.
12. Knochel, T., et al., and Jansonius, J.N. (1999). The crystal structure of anthranilate synthase from Sulfolobus solfataricus: functional implications. Proc. Natl. Acad. Sci. USA *96*, 9479–9484.
13. Chittur, S.V., Klem, T.J., Shafer, C.M., and Davisson, V.J. (2001). Mechanism for acivicin inactivation of triad glutamine amidotransferases. Biochemistry *40*, 876–887.
14. Beismann-Driemeyer, S., and Sterner, R. (2001). Imidazole glycerol phosphate synthase from *Thermotoga maritima*: quaternary structure, steady-state kinetics and reaction mechanism of the bi-enzyme complex. J. Biol. Chem. *276*, 20387–20396.
15. Lang, D., Thoma, R., Henn-Sax, M., Sterner, R., and Wilmanns, M. (2000). Structural evidence for evolution of the beta/alpha barrel scaffold by gene duplication and fusion. Science *289*, 1546–1550.
16. Fani, R., et al., and Polsinelli, M. (1997). Paralogous histidine biosynthetic genes: evolutionary analysis of the *Saccharomyces cerevisiae his6* and *his7* genes. Gene *197*, 9–17.
17. Ollis, D.L., et al., and Goldman, A. (1992). The α/β hydrolase fold. Protein Eng. *5*, 197–211.
18. Thoden, J.B., Miran, S.G., Phillips, J.C., Howard, A.J., Raushel, F.M., and Holden, H.M. (1998). Carbamoyl phosphate synthetase: caught in the act of glutamine hydrolysis. Biochemistry *37*, 8825–8831.
19. Thoden, J.B., Huang, X., Raushel, F.M., and Holden, H.M. (1999). The small subunit of carbamoyl phosphate synthetase: snapshots along the reaction pathway. Biochemistry *38*, 16158–16166.
20. Hodel, A., Kim, S.H., and Brünger, A.T. (1992). Model bias in macromolecular crystal structures. Acta Crystallogr. A *48*, 851–858.
21. Franco, M.G., Laber, B., Huber, R., and Clausen, T. (2001). Structural basis for the function of pyridoxine 5′-phosphate synthase. Structure *9*, 245–253.
22. Hennig, M., Darimont, B., Sterner, R., Kirschner, K., and Jansonius, J.N. (1995). 2.0 Å structure of indole-3-glycerol phosphate synthase from the hyperthermophile *Sulfolobus solfataricus*: possible determinants of protein stability. Structure *3*, 1295–1306.
23. Branden, C.-I. (1991). The TIM barrel—the most frequently occurring folding motif in proteins. Curr. Op. Struct. Biol. *1*, 978–983.
24. Wilmanns, M., Hyde, C.C., Davies, D.R., Kirschner, K., and Jansonius, J.N. (1991). Structural conservation in parallel beta/alpha-barrel enzymes that catalyze three sequential reactions in the pathway of tryptophan biosynthesis. Biochemistry *30*, 9161–9169.
25. Bork, P., Gellerich, J., Groth, H., Hooft, R., and Martin, F. (1995). Divergent evolution of a beta/alpha-barrel subclass: detection of numerous phosphate-binding sites by motif search. Protein Sci. *4*, 268–274.
26. Mancia, F., et al., and Evans, P.R. (1996). How coenzyme $B_{12}$ radicals are generated: the crystal structure of methylmalonyl-coenzyme A mutase at 2 Å resolution. Structure *4*, 339–350.
27. Hocker, B., Beismann-Driemeyer, S., Hettwer, S., Lustig, A., and Sterner, R. (2001). Dissection of a $(\beta/\alpha)_8$-barrel enzyme into two folded halves. Nat. Struct. Biol. *8*, 32–36.
28. Otwinowski, Z., and Minor, W. (1997). Processing of X-ray diffraction data collected in oscillatin mode. In Methods in Enzymology, Volume 276, C.W. Carter, Jr. and R.M. Sweet, eds. (New York: Academic Press), pp. 307–326.
29. Terwilliger, T.C., and Berendzen, J. (1999). Automated structure solution for MIR and MAD. Acta Crystallogr. D *55*, 849–861.
30. CCP4 (Collaborative Computational Project 4) (1994). The CCP4 suite: programs for protein crystallography. Acta Crystallogr. D *50*, 760–763.
31. Jones, T.A., Zou, J.Y., Cowan, S.W., and Kjeldgaard, M. (1991). Improved methods for binding protein models in electron density maps and the location of errors in these models. Acta Crystallogr. A *47*, 110–119.
32. Brünger, A.T., et al., and Warren, G.L. (1998). Crystallography and NMR system (CNS): a new software system for macromolecular structure determination. Acta Crystallogr. D *54*, 905–921.
33. Lewis, R.M., Nancollas, G.H., and Coppens, P. (1972). The crystal and molecular structure of [N,N'-di(2-aminoethyl)malondiamidato]nickel (II) trihydrate. Inorg. Chem. *11*, 1371–1375.
34. Kleywegt, G.J., and Jones, T.A. (1997). Model-building and refinement practice. In Methods in Enzymology, Volume 277, C.W. Carter, Jr. and R.M. Sweet, eds. (New York: Academic Press), pp. 208–230.
35. Laskowski, R.A., MacArthur, M.W., Moss, D.S., and Thornton, J.M. (1993). PROCHECK: a program to check the stereochemical quality of protein structures. J. Appl. Crystallogr. *26*, 283–291.
36. Hubbard, S.J., and Thornton, J.M. (1993). NACCESS, Computer Program, Department of Biochemistry and Molecular Biology (London: University College London).
37. Nicholls, A., Sharp, K.A., and Honig, B. (1991). Protein folding and association: insights from the interfacial and thermodynamic properties of hydrocarbons. Proteins Struct. Funct. Gen. *11*, 282.
38. Thompson, J.D., Higgins, D.G., and Gibson, T.J. (1994). CLUSTAL W: improving the sensitivity of progressive multiple sequence alignment through sequence weighting, position-specific gap penalties and weight matrix choice. Nucleic Acids Res. *22*, 4673–4680.
39. Kleywegt, G.J., and Jones, T.A. (1994). Detection, delineation, measurement and display of cavities in macromolecular structures. Acta Crystallogr. D *50*, 178–185.
40. Vriend, G., and Sander, C. (1993). Quality control of protein models: directional atomic contact analysis. J. Appl. Crystallogr. *26*, 47–60.
41. Kabsch, W., and Sander, C. (1983). Dictionary of protein secondary structure: pattern recognition of hydrogen-bonded and geometrical features. Biopolymers *22*, 2577–2637.
42. Kraulis, P. (1991). Molscript. A program to produce both detailed and schematic plots of protein structures. J. Appl. Crystallogr. *24*, 946–950.
43. Esnouf, R.M. (1999). Further additions to MolScript version 1.4, including reading and contouring of electron-density maps. Acta Crystallogr. D *55*, 938–940.
44. Merritt, E.A., and Bacon, D.J. (1997). Raster3D: photorealistic molecular graphics. In Methods in Enzymology, Volume 277, C.W. Carter, Jr. and R.M. Sweet, eds. (New York: Academic Press), pp. 505–524.

## Accession Numbers

The final model and diffraction data are deposited in the Protein Data Bank under ID code 1JVN.